POLITECNICO DI TORINO
Repository ISTITUZIONALE

Experimental investigation on the turbulence flame autoignition characteristics of ammonia in a high-temperature co-flow

Original
Experimental investigation on the turbulence flame autoignition characteristics of ammonia in a high-temperature co-flow / Ji, M., Wu, Z., Ferrari, A., Vento, O., Shang, Q., Zhang, G., Fu, L., Deng, J., Li, L.. - In: FUEL. - ISSN 0016-2361. - 372:(2024). [10.1016/j.fuel.2024.132216]

Availability:
This version is available at: 11583/2989861 since: 2025-02-05T13:08:56Z

Publisher:
Elsevier

Published
DOI:10.1016/j.fuel.2024.132216

Terms of use:

This article is made available under terms and conditions as specified in the corresponding bibliographic description in the repository

Publisher copyright
Elsevier postprint/Author's Accepted Manuscript

© 2024. This manuscript version is made available under the CC-BY-NC-ND 4.0 license
http://creativecommons.org/licenses/by-nc-nd/4.0/.The final authenticated version is available online at:
http://dx.doi.org/10.1016/j.fuel.2024.132216

(Article begins on next page)

18 November 2026

Experimental investigation on the turbulence flame autoignition characteristics of ammonia in a high-temperature co-flow

Meng Ji[ab], Zhijun Wu[a*], Alessandro Ferrari[b*], Oscar Vento[b], Quanbo Shang[a], Guanyu Zhang[a], Lezhong Fu[c], Jun Deng[a], Liguang Li[a]

a School of Automotive Studies, Tongji University, Shanghai, China

b Energy Department, Politecnico di Torino, Turin, Italy

c United Automotive Electronic Systems Co., Ltd., Shanghai, China

(*) Corresponding Authors

Abstract

Ammonia has a promising future for transportation and industrial power as an innovative zero-carbon fuel because of the harsh emission laws in force and the pressing need of low carbon fuels. Thus, the aim of this work has been to investigate the autoignition characteristics of an ammonia turbulence flame under a high co-flow temperature, on the basis of an experimental platform. The morphology, lift height, and stability of an ammonia jet diffusion flame have been explored under different co-flow regimes (in terms of temperature and velocity) and fuel injection pressures. It was found that when the co-flow temperature augments, the ammonia jet can form a stable lifting flame. Moreover, the combustion stability of the ammonia flame increases significantly and the fluctuation of the lift height of the flame clearly decreases over time. Forming a stable ammonia jet lifting flame under high co-flow velocities and injection pressures requires a high co-flow temperature. The length, area, and perimeter of an ammonia jet diffusion combustion flame increase as the co-flow temperature increases. The distance from the point of autoignition to the central nozzle outlet and the ignition delay both decrease when the co-flow temperature augments. The lift height of an ammonia diffusion combustion flame gradually decreases as the co-flow temperature increases. Moreover, there is a critical temperature of 1173 K beyond which the decline slope of both the lift height and ignition delay decreases.

1. Introduction

The traditional internal combustion engine industry is currently in a position where it has to develop clean energies to cope with the increasingly stringent emission regulations of internal combustion engines and to satisfy the zero-carbon policy requirements. The application of and research into

zero-carbon fuels have become the main directions for future developments. Ammonia is a new type of low-cost zero-carbon fuel. It can be derived from diverse sources, including traditional fuels such as coal, natural gas, and oil, as well as waste heat, hydropower, urban waste, and various biomass wastes [1]. Ammonia can also be produced from renewable energy sources, such as solar energy, wind energy, geothermal energy and marine energy, for completely carbon-free synthesis [2]. Ammonia has been used in industry for more than a century, and its production, storage, and transportation are more complete and mature than other zero-carbon fuels, such as hydrogen. Moreover, because of its relatively mature level of technology, should ammonia be used as a new type of energy in the future, the investment costs will be affordable [3]. Compared with hydrogen, ammonia features valuable storage properties. Indeed, the liquefaction temperature of ammonia is much higher than that of hydrogen, thus opening the way toward the possibility of diminishing the storage pressure. A lower storage pressure and volume could reduce the storage and transportation costs, which are about 10 times and 45 times lower, respectively, than the corresponding ones for hydrogen [4].

Back in 1965, General Motors investigated the use of ammonia as a fuel for a single-cylinder spark ignition (SI) engine to free the Armed Forces from reliance on hydrocarbon fuels [5]. Comparing the obtained results with those obtained for gasoline, under similar working conditions, they revealed losses in power and thermal efficiency, due to the inability of the engine to burn ammonia efficiently (as deducted from the large amount of ammonia detected in the exhaust gases). More studies were performed in the mid-60s to assess the compatibility of ammonia with the materials and lubricants used for the manufacturing of internal combustion engines [6], and no serious problems were noted. Different studies have been conducted over the last two decades to explore the applicability of ammonia as a fuel for SI engines, for different compression ratio (CR) values, engine speeds, ammonia amounts and fuel promoters [7-9]. In [10], an SI engine was tested with CR=10.5, and it resulted that the engine could only work under a very low load for a 10% addition of H_2 to promote the ignition of the fuel mixture. On the other hand, the high-octane number (>130) [11] of ammonia helps to improve thermal efficiency, thereby allowing high CR values to be used [12].

There are evident difficulties involved in igniting ammonia, due to its high ignition temperature (651 °C) and a narrow ignition range [13]. Furthermore, ammonia may suffer from unstable

61 combustion phenomena, such as misfire and flashback, and these have been ascribed to the low
62 laminar speed of the flame [14]. Despite the abovementioned challenging factors, ammonia also
63 represents a promising fuel for compression ignition (CI) engines, due to their elevated CR, even
64 though the dual-fuel operating condition seems to be the most suitable for light CI engines employed
65 in the transport sector. The impact of replacing diesel fuel with ammonia in an ammonia/diesel dual-
66 fuel engine was studied in [15], and the results showed that up to 84.2% of the input energy can be
67 provided by ammonia. However, since, in this case, the ammonia was injected into the intake port,
68 a reduced compression pressure was reached (the ammonia heat capacity ratio was lower than that
69 of air) and the oxygen concentration in the cylinder diminished (it was difficult for the diesel pilot
70 shot to mix with air and ignite). These two effects, together with the elevated minimum ignition
71 energy of ammonia, led to a delayed start of combustion, compared with that obtainable under a
72 pure diesel working condition.
73 Ammonia-diesel stratified injection was numerically explored for a marine low-speed engine in [16].
74 The diesel fuel, the injection of which occurred before that of the ammonia (both fuels were injected
75 through a dual-fuel DI concentric injector), started to burn because of its short chemical ignition
76 delay: the ammonia close to the combustion area reached an autoignition condition and diffusive
77 combustion started. The results obtained for an injection pressure of 700 bar showed that the ignition
78 delay time in the dual-fuel mode was reduced, compared with the pure diesel working condition,
79 due to the rapid evaporation of ammonia (short physical ignition delay), which contributed to a
80 faster premixing with air, thus reaching a minimum ignition delay value when the diesel energy
81 share was 5%. A CI engine, in which premixed ammonia was used together with an n-heptane pilot
82 shot, was also tested in [17]. Because of its reduced kinematic viscosity, compared with diesel, the
83 addition of n-heptane allowed very small pilot injections and reduced spray droplets to be obtained
84 for the adopted GDI injector (the injection pressure was fixed at 120 bar). It was seen that the
85 ammonia combustion efficiency increased together with the NH_3 fuel energy-share (the latter was
86 varied between 80% and 98.5%). In fact, it was observed that the higher the amount of ammonia of
87 the energy-share was, the lower the local air-to-fuel ratio that approached the stoichiometric value,
88 and the higher the ignition capability of the fuel mixture.
89 The combustion of an ammonia/DME mixture in a CI engine was investigated in [18]. DME was
90 employed to initiate the combustion and, thanks to its polarity, it formed a stable mixture with

ammonia; furthermore, since these fuels are characterized by a high vapor pressure, both required pressurization to remain in a liquid state. The results of a direct fuel injection strategy showed that a stable combustion was only achieved for the highest ammonia energy-share (40%) by increasing the fuel injection pressure to 180 bar in order to enhance fuel mixing and atomization, while 150 bar was enough for an ammonia energy-share of up to 20%. A higher energy share of ammonia could be reached by increasing the injection pressure [18]; this should not be an issue, considering the elevated injection pressure levels modern diesel Common Rail injection systems [19-22] or GDI ones [23] feature.

Many researchers have analyzed the ignition delay [24, 25], flammability limits, and combustion stability of ammonia [26]. Karan explored the laminar flame speed of ammonia at temperatures of 300-600 K and under a pressure in the 2-37 bar range, and determined a new set of constants for the evaluation of the laminar flame speed [27]. The experimental results reported in [28] showed that the maximum value of the unstretched laminar burning velocity was below 7 cm/s, that is, lower than those of hydrocarbon flames.

Most of the research on ammonia fuel has focused on spherical (laminar) flames [29, 30], and studies on the combustion characteristics of the turbulent jet flame of ammonia fuel at high temperatures has still not been explored in great depth to guide the development of ammonia engines. Some researchers have explored the turbulent flame combustion characteristics of ammonia. In [31], the ammonia turbulent flame propagation speed was measured under oxygen-enriched air conditions, and it was found that lean mixtures were affected more by diffusional instability effects because the mass diffusion of the reactants from the unburned area to the burned one was different from the thermal diffusion from combustion products to reactants (the Lewis number was different from 1). These, together with turbulence eddies, induced a higher turbulent burning velocity. Kobayashi showed that the turbulent methane flame of ammonia resulted in an increased scale of the wrinkled flame front, because of the increased flame thickness of ammonia [32]. In [33], the authors found, by means of direct numerical simulations, that the high heat release rate and NO formation for ammonia/hydrogen blends occurred in correspondence to concave structures of the flame, and lean mixtures showed high turbulent burning velocity values.

The experimental research on the autoignition characteristics of an ammonia turbulence jet with a high temperature co-flow and of the subsequent combustion development is essential to explain the

diffusive combustion characteristics of ammonia and to support the design of ammonia CI engines. A controlled thermal atmosphere burner (Dibble burner [34,35]) is widely used, and it allows the cause-and-effect relationships between a turbulent flow and chemical reactions to be simplified and investigated. A vitiated co-flow flame is a turbulent flow that reacts within a hot environment, but it has a simplified geometry. A jet of ammonia enters a co-flow of hot combustion products of a lean premixed flame. The large diameter of the co-flow leads the central fuel jet to be isolated from the environment, and the fluid domain may therefore be simplified as a two-stream flow. A wide range of experimental research has been conducted with the Dibble burner on H_2/N_2[36], H_2/CO_2[37], $H_2/Ar/O_2$ [38] and methane [39].

In this work, ammonia diffusive jet flames have been investigated experimentally in a high-temperature and environment pressure co-flow. The combustion characteristics of the ammonia fuel jet were measured by means of a controlled thermal atmosphere burner. The morphology of the combustion jet flame was examined through an extensive experimental campaign on different co-flow velocities, co-flow temperatures, and ammonia jet velocities. Furthermore, a quantitative analysis was performed concerning the flame stability of a non-premixed ammonia jet and the auto-ignition combustion properties under high temperature conditions, and the influence of the co-flow temperature on both the length of the normalized lift-off and the ignition delay was analyzed. The results of this study can thus be considered as an experimental basis to evaluate and improve combustion models and for the subsequent analysis of ammonia diffusive combustion in a high-pressure and high-temperature co-flow.

2. Experimental design

2.1 Introduction of the experimental ammonia jet flame combustion device

The test system used for the ammonia fuel combustion experiments is reported in Figure 1, and it is made up of five parts: the main body of the controllable thermal-atmosphere burner, the co-flow control system, the ammonia jet control system, the cooling system, and the data acquisition system. The main element is the controllable thermal-atmosphere burner: it generates a stable co-flow temperature field for ammonia jet combustion. The combustion disk was manufactured with a porous structure. The co-flow premixed gas passes through the porous combustion disk and is ignited above the latter to form countless small premixed laminar flow flames, thus constituting a flat laminar flame that builds a stable high-temperature atmosphere for the jet flame. The porous

disk has 874 uniformly distributed 1.2 mm diameter small holes, and the centers of the holes are located 3 mm from each other.

The co-flow control system manages both the temperature and the speed of the co-flow field. The former can be varied by acting on the amount of hydrogen in the co-flow, while the latter can be adjusted by means of a blower (cf. Figure 1). The co-flow temperature is measured by means of a thermocouple, and it is used as a feedback signal that acts on the hydrogen pressure reducing value (item 1 in Figure 1) to reach the desired target co-flow temperature value. In order to minimize the interference of the jet combustion on the thermocouple, the latter is arranged at a certain distance from the ammonia injector. The thermocouple was installed on a three-dimensional moving platform to verify the uniformity of the co-flow temperature field, and the temperature was measured at different locations. The temperature is recorder 30 seconds after the thermocouple is moved to allow the thermal regime to be reached. Autoignition occurs for all the considered experimental conditions in the verified uniform part of the co-flow field, which consists of a cylinder with a diameter of around 90 mm and a height of around 180 mm.

The co-flow velocity is determined on the basis of the volumetric flowrate of the blower (measured at T= 20 °C and p=1 atm), and the corresponding mass flowrate can be calculated. The co-flow velocity can then be determined by imposing the mass conservation law, since the burner is exposed to the environment, and by knowing both the burner cross section area (determined on the basis of the diameter of the burner) and the co-flow density, the latter of which is determined by means of the perfect gas law with the measured co-flow temperature (a static pressure equal to 1 atm is considered). The air properties were used to determine the co-flow velocity (R= 287 J/kgK, γ=1.4) for each set of air volumetric flowrate and co-flow temperature, because of the great excess of the air flowrate compared to the hydrogen one. Figure 2 reports the co-flow velocities for different temperatures and for fixed values of the volumetric flowrates of the blower. As can be inferred from Figure 2, the co-flow velocity is mainly controlled by the flowrate of the blower. However, the co-flow velocity is also a function of the co-flow temperature for a fixed blower flowrate (since the co-flow pressure is fixed, the density reduces when the temperature augments) and such a temperature is increased by augmenting the hydrogen flowrate.

The jet control system includes a central injector pipe with an inner diameter, d, of 6.5 mm, an ammonia tank, a solenoid valve, a pressure regulating valve, and a mass flowmeter. The liquid

ammonia tank, which is made of stainless steel, is equipped with a pressure gauge with a maximum pressure of 12 bar. When the ammonia pressure reaches the injection pressure (which is controlled by means of a device placed between the ammonia tank and the injector), ammonia is in a gas state, and a solenoid valve, equipped with an LH-04 relay module, opens to start the injection. In order to realize synchronization between the ammonia injection and the high-speed camera, the LH-04 relay module was used to control the two signals at the same time, so that the high-speed camera could receive a 5 V high level signal to begin simultaneously recording with the fuel injection.

The cooling system is constituted by two water channels, one for the injection tube (not reported in Figure 1), and the other for the outer side of the burner. A high-speed camera, which was used to collect the ammonia fuel combustion experimental data, is included in the data acquisition system.

Table 1 reports the test conditions in terms of the co-flow velocity (u_{cf}), injection pressure (p_{inj}), the corresponding injection velocity (u_{inj}), and the co-flow temperature (T_{cf}). The ammonia pressure range was selected in order to explore the transition from a laminar to turbulent flow regime: in fact, if $p_{inj} \leq 1.6$ bar, the flow is laminar or in a transitional regime with a Reynolds number equal to $Re=\rho_{inj}u_{inj}d/\mu_{inj}<5000$, where $\mu_{inj}=9.83\cdot10^{-6}$ Pa·s is the dynamical viscosity of ammonia and ρ_{inj} indicates the ammonia density, while the flow is in a turbulent regime ($Re<15000$) if $p_{inj}\geq1.9$ bar. The co-flow velocity and temperature values guarantee a turbulent regime ($Re>>2000$) for all the conditions, as usually occurs in the combustion chamber of a CI engine. As can be inferred from Figure 2, the co-flow temperature only affects the co-flow velocity slightly and is mainly controlled by the flowrate of the blower. Therefore, for conciseness reasons, in what follows, we refer to a mean value of the co-flow velocity, averaged over the temperatures, for each blower flowrate (cf. in Table 1).

Table 1. Experimental conditions.

Co-flow velocity (u_{cf}) [m/s]	23, 25, 27, 29, 32, 34
Injection pressure (p_{inj}) [bar]	1.3, 1.6, 1.9, 2.2, 2.5
Injection velocity (u_{inj}) [m/s]	3.6, 10.2, 16.8, 23.4, 29.9
Co-flow temperature (T_{cf}) [K]	1113-1223

As far as the evaluation of u_{inj} is concerned, the presence of a water layer around the fuel pipe makes the heat transfer from the co-flow to the fuel virtually null during the working conditions of the burner. The outlet velocity of the fuel jet can be determined by assuming that its temperature is

almost equal to the water-cooling temperature. Therefore, the velocity of the ammonia jet was determined for each tested p_{inj}, on the basis of the measured fuel mass flow-rate, the pipe cross section area, and the fuel density (the density of the ammonia was calculated under environment pressure and for the water-cooling temperature).

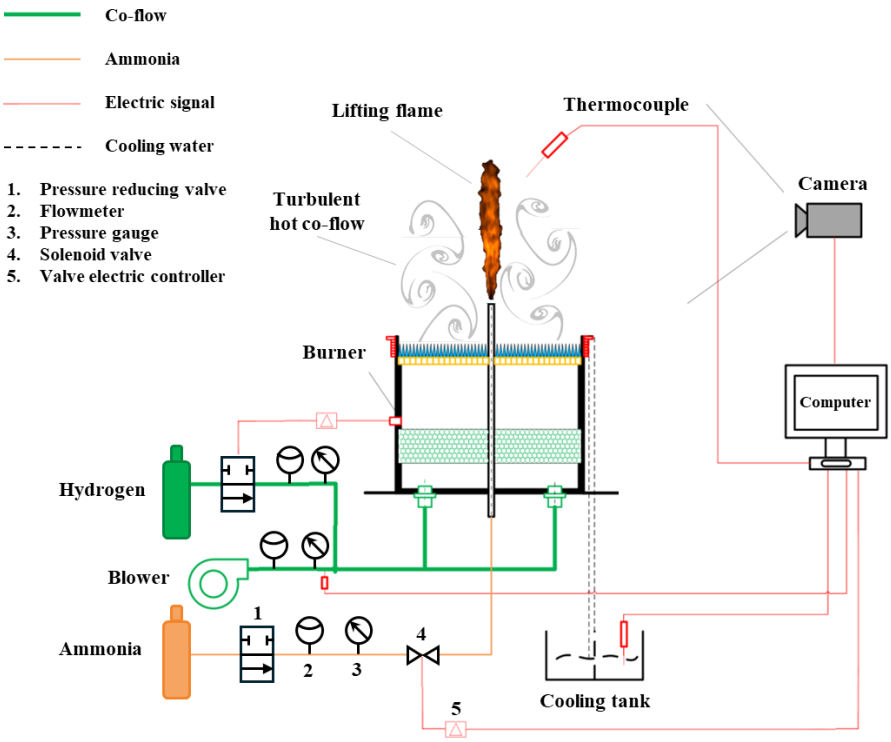


Figure 1. Ammonia fuel combustion test system.

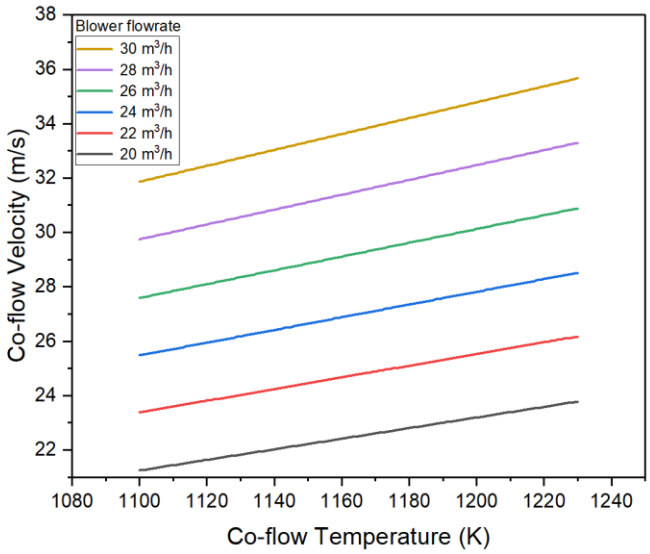


Figure 2 Co-flow velocities for different temperatures and blower flowrates.

Table 2 reports the compositions of the co-flows, determined by means of CHEMKIN software with the GRI-Mech 3.0 mechanism [40] and corresponding to the reported T_{cf} values (Y stands for the

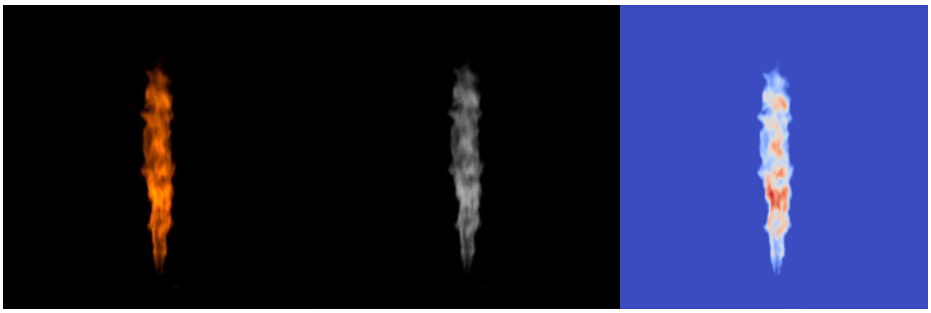
mass fraction). As can be inferred, when the co-flow temperature increases, the H_2O concentration, namely Y_{H20}, augments slightly, while the nitrogen and oxygen mass fractions reduce slightly (the Y_{02} reduction is around 5% whenever the co-flow temperature passes from 1123 K to 1223 K).

T_{cf}	Y_{H2O}	Y_{N2}	Y_{O2}
1123 K	0.071	0.761	0.168
1148 K	0.074	0.761	0.165
1173 K	0.076	0.76	0.164
1198 K	0.079	0.76	0.161
1223 K	0.081	0.76	0.159

Table 2. Co-flow compositions for different co-flow temperatures.

2.2 The data processing method

The image data extraction program is compiled of Python software to batch-process the flame images of the turbulent jet of the ammonia fuel under different conditions. The main steps of the image data extraction algorithm are shown in Figure 3 and can be summarized as follows: the original flame image is acquired by the camera (cf. Figure 3a); a grayscale flame image (cf. Figure 3b) and a colored flame image (cf. Figure 3c) are obtained; the appropriate threshold for image binarization (cf. Figure 3d) is obtained by reducing the difference between the morphology of the original flame picture (Figure 3a) and the one given by the binarization (Figure 3d). Finally, the contour information and the characteristic parameters, such as the lift height, the flame length, the flame area, and the perimeter of the flame, are obtained (cf. Fig 3e).



(a) Original figure (b) Grayscale (c) Colored grayscale



(d) Binarization (e) Flame data extraction

Figure 3. Data processing method.

The extracted characteristic parameters are shown in Figure 4 (the horizontal dashed line represents the position of the fuel pipe outlet). The normalized flame lift height can be computed by measuring the distance between the lowest point of the extracted jet flame and the injection outlet, denoted as *H*, as the *H/d* ratio, where *d* represents the inner diameter of the fuel pipe. The flame length, labeled *L*, is defined as the distance between the highest and lowest points of the extracted flame. Moreover, the flame perimeter is represented by the length, *C,* of the extracted flame edge. Lastly, the flame area, denoted as *S*, is the area enclosed by this edge, and the flame area-to-perimeter ratio is defined as *S/C*. Since steady-state flames should be considered, 20-50 consecutive flame pictures with a visible flame were selected for the experimental analysis, and the average value of each parameter was calculated as the characteristic parameter of the flame, under certain conditions, to ensure the reliability of the data. The camera has a resolution of 512×512 pixels, a shooting frequency of 500 Hz, and an exposure time of 2 ms.

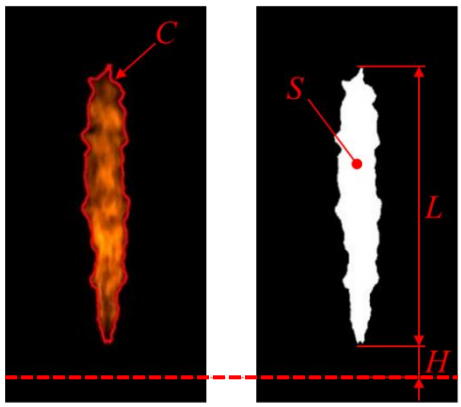


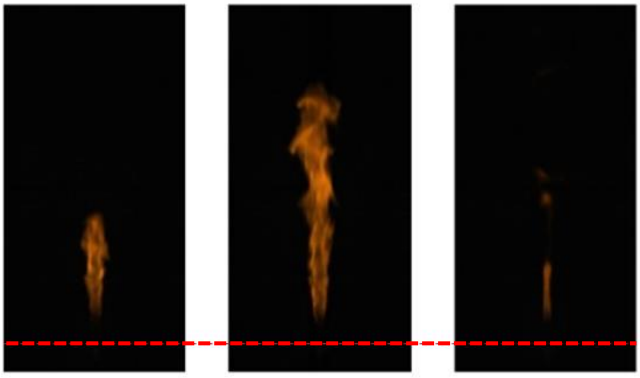
Figure 4. Schematic diagram of the characteristic parameters of the jet flame.

3. The diffusion combustion characteristics of ammonia

3.1 Characteristics of the ammonia jet flame morphology

Figure 5 shows the ammonia diffusion and autoignition process in the co-flow field captured by the high-speed camera under the conditions of T_{cf}= 1223 K, u_{cf} = 25 m/s, and p_{inj}= 1.9 bar. The development process of the jet flame is mainly divided into the following stages: 1) the explosion-proof solenoid valve for the ammonia injection into the high-temperature co-flow field is opened; 2) the ammonia jet mixes with air and starts to spontaneously ignite in the high-temperature co-flow field (cf. Figure 5a); 3) and, after autoignition of the ammonia jet, the flame length, flame area, and flame brightness increase rapidly and a stable lifting flame is formed (cf. Figure 5b); 4) after a stable lifting flame of the ammonia jet forms, the flame lasts for a period of time that is mainly determined by the pulse width of the solenoid valve of the ammonia jet; 5) at the end of the ammonia injection, the amount of residual fuel quickly diminishes, and the jet flame is gradually extinguished until the leftover fuel is completely burned (cf. Figure 5c). The considered definition of ignition delay takes into account the time interval between the opening of the solenoid valve, which leads to the start of injection of the ammonia, and the observation of the initial autoignition of the fuel jet.

The ammonia jet diffusion flame is orange, in agreement with [41, 42]: the main reason for the formation of this flame is the spectrum of the NH_2 free radicals and water vapor in the ammonia flame. According to the images of the development of the ammonia jet flame and the continuous combustion of the lifting flame taken by the high-speed camera, it can be seen that the ammonia jet presents clear turbulent flame corrugation characteristics.



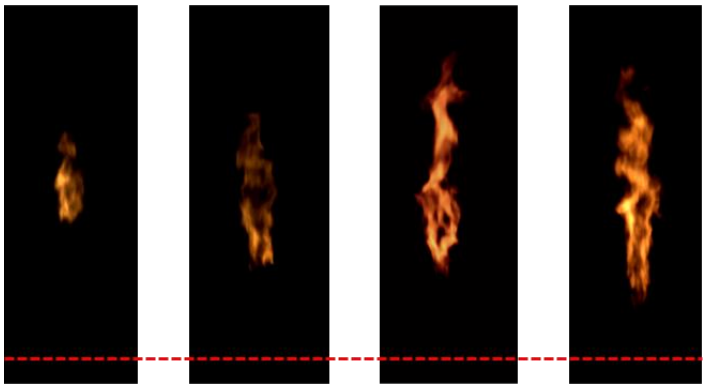
(a) autoignition (b) combustion (c) extinction

Figure 5. Ammonia diffusion combustion in the co-flow field captured by the high-speed camera.

Figure 6a shows the flame characteristics of an ammonia jet, for different T_{cf}, under the conditions

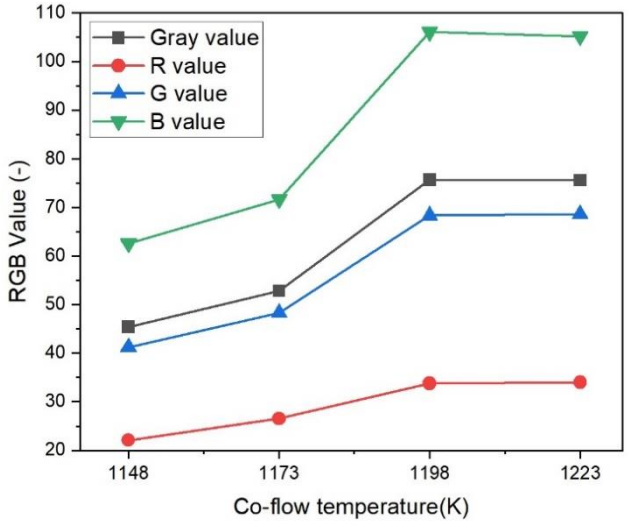
of u_{cf} = 25 m/s, and p_{inj}= 1.9 bar, while Figure 6b reports the brightness of the flame (averaged over the entire flame surface), quantified by means of the R, G, and B values, and the corresponding grayscale value (given by $0.299 \cdot R + 0.587 \cdot G + 0.114 \cdot B$). It can be seen that when the co-flow temperature increases, the ammonia flame becomes lighter and longer, the overall injected ammonia can burn, and combustion becomes more complete and stable. Data referring to a T_{cf} value below 1123 K are not reported since the high-speed camera was not able to capture the ammonia jet flame because of its low brightness level. The overall brightness of the flame is low for a T_{cf} value of 1148 K, and the length of the flame is also significantly reduced. In this case, the combustion results to be unstable (the flame is sometimes visible and sometimes not), due to the low T_{cf} value. This is evident from Figure 6c, which represents the history of the flame area time during fuel injection: a flame is formed at the beginning for T_{cf}=1148 K, but it is rapidly extinguished. Combustion becomes more stable for higher co-flow temperatures (the sum of the time intervals over which the flame area is higher than zero augments), and the flame can be detected throughout the entire fuel injection time interval for T_{cf}≥1198 K. When T_{cf} reaches 1223 K, the brightness of the orange flame is significantly enhanced (cf. Figures 6a and 6b), because the high temperature makes the high vibrational excited states of the molecule in the ammonia flame more pronounced. The effects of different co-flow velocities and jet pressures on the stability and characteristic parameters of an ammonia flame were investigated considering the different characteristics of the ammonia flame under different T_{cf} values, and that ammonia cannot form a stable lifting flame under low T_{cf}.

Figure 6d shows characteristic images of the ammonia jet flames for different jet velocities under the conditions of T_{cf}=1173 K and a co-flow velocity equal to 25 m/s. It can be seen that the lift height of the flame generally increases as the injection pressure increases. However, when p_{inj} reaches 2.5 bar, the overall brightness of the flame is lower than that at 2.2 bar and the flame length is significantly lower, which indicates that the autoignition of the ammonia jet is unstable. This is due to the large amount of ammonia injected into the co-flow field, which makes the local equivalence ratio become richer. The finite co-flow field limits both the heat exchange and the mixing, thus making it more difficult for ammonia to form a stable flame in such a rich fuel condition. This is why the maximum injection pressure was selected as 2.5 bar.

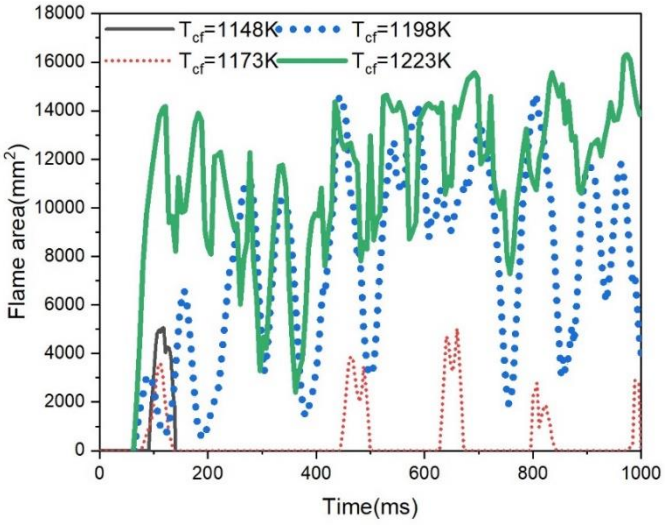


1148 K 1173 K 1198 K 1223 K

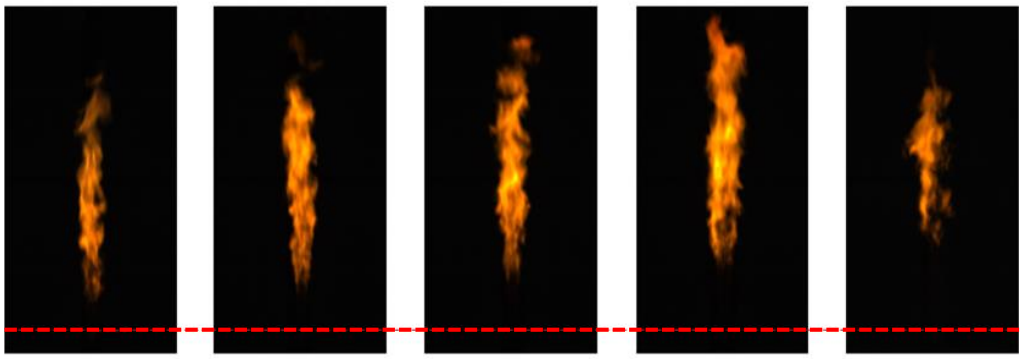
a. Pictures of ammonia jet flames for different co-flow temperatures (u_{cf} = 25 m/s, p_{inj} =1.9bar)



b. Averaged R, G, B and gray values of an ammonia flame for different co-flow temperatures (u_{cf} = 25 m/s, p_{inj} =1.9bar)



c. Time histories of the flame area for different co-flow temperatures (u_{cf} = 25 m/s, p_{inj} =1.9bar)



1.3 bar 1.6 bar 1.9 bar 2.2 bar 2.5 bar

d. Pictures of ammonia jet flames for different injection pressures (u_{cf} = 25 m/s, T_{cf} =1173 K).

Figure 6. Pictures of the brightness and stability of ammonia jet flames.

3.2 Study of the autoignition combustion boundary

Figure 7 shows the autoignition temperature of ammonia for different co-flow velocities for p_{inj}=1.9 bar. Three to five independent experiments were used for each condition to determine the combustion boundary. The blue triangles in Figure 7 represents stable combustion, which means the flame was always observed for those conditions (in terms of u_{cf} and T_{cf}), and the black squares represent the autoignition boundary for each co-flow velocity value, which means that the flame was sometimes recorded (cf. the curve for T_{cf}= 1173 K in Figure 6c), while a red circle denotes a condition for which the ammonia jet could not be autoignited. According to the experimental results of the different co-flow velocities reported in Figure 7, the autoignition temperature boundary of the ammonia jet increases as the co-flow speed increases. For example, if we consider a co-flow speed of 23 m/s, it can be seen that the ammonia jet can be autoignited at a co-flow temperature beyond 1163 K and form a stable lifting flame. Similarly to Figure 7, Figure 8 shows the autoignition combustion temperature of ammonia for different p_{inj} and for a fixed co-flow velocity equal to 25 m/s. According to the experimental results of different jet pressures, the autoignition temperature boundary of the ammonia jet increases as the jet pressure increases. For example, if p_{inj}=1.6 bar, the ammonia jet can autoignite when the co-flow temperature is beyond 1158 K and form a stable lifting flame. A higher injection pressure for the same co-flow temperature leads to a higher initial momentum and a higher jet velocity. A higher jet velocity reduces both the mixing time between the ammonia and the co-flow and the time available to absorb energy from the co-flow, and the ammonia

therefore cannot reach the autoignition temperature. The dashed lines in Figures 7 and 8 denote the boundaries of the co-flow temperature above which autoignition can be achieved for each co-flow velocity and injection pressure, respectively. Experimental tests to determine the autoignition conditions reported in Figures 7 and 8 have been repeated three times, and coincident results have been obtained.

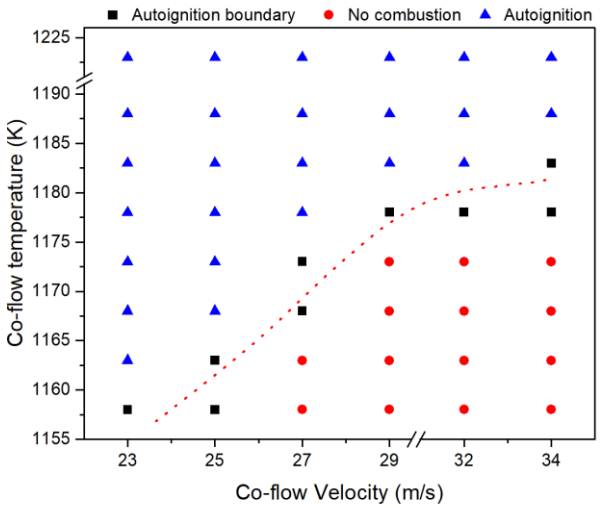


Figure 7. Autoignition of ammonia for different co-flow velocities (p_{inj}=1.9 bar).

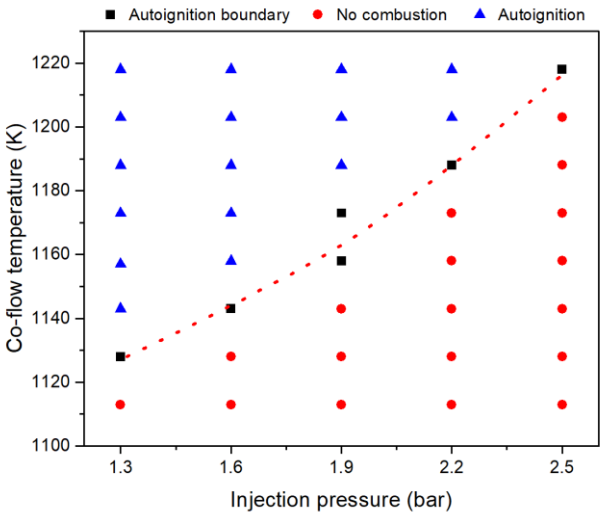


Figure 8. Autoignition of ammonia gas for different jet pressures (u_{cf} = 25 m/s).

3.3 Characteristic parameters of the flame

The length and area of the flame are reported in Figure 9 for different co-flow temperatures, while Figure 10 shows the corresponding perimeter and aspect ratio, *S/C,* of the flame. In both figures, u_{cf} has been kept constant at 25 m/s, and p_{inj} is equal to 1.9 bar. Data concerning two different

acquisitions have been reported, showing a satisfactorily repeatability. As can be inferred from Figures 9 and 10, the length, area, perimeter, and aspect ratio of the ammonia flame increase as T_{cf} increase. The length of the ammonia combustion flame is primarily affected by the flame speed of ammonia. If T_{cf} is increased, the flame speed of ammonia augments [43], thus promoting a faster development of the ammonia flame in the axial direction. Therefore, the diffusion ability of ammonia becomes stronger for an increment of the T_{cf} value, and this leads to an augmented flame area. The flame perimeter also increases together with the value of T_{cf}, due to the more pronounced flame length and wrinkle.

When the flame length is mainly regulated by the initial jet momentum [44], it is positively correlated with the ratio of the jet density (ρ_{inj}) to the co-flow density (ρ_{cf}), according to the following law [38]:

$$L \propto \left(\frac{\rho_{inj}}{\rho_{cf}}\right)^{0.5} \qquad (1)$$

The dashed curve plotted in Figure 9, which is based on Eq. (1), was determined from experimental data of co-flow temperatures of up to 1198 K. Indeed, an asymptotic flame length value exists for a certain value of the initial axial jet momentum, i.e. a fixed fuel flow rate: such a value is reached as the fuel jet is able to absorb enough heat from the co-flow to ensure complete combustion. A knee can be observed to have occurred in Figure 9 when T_{cf}=1198 K, and the flame length for T_{cf}>1198 K starts to be less sensitive to T_{cf}, while any further increment only reduces the lift-off length.

As can be inferred from Figures 9 and 10, the geometrical features of the flame augment slightly when the co-flow temperature goes beyond 1198 K: this means that, when T_{cf}=1198 K, u_{cf}= 25 m/s, p_{inj}=1.9 bar, the fuel jet is already capable of absorbing the required energy from the co-flow field for a complete combustion process, and only marginal modifications in the flame structure can therefore be recognized for a further increment in the co-flow temperature. This result is in line with other results available in the literature concerning hydrogen-argon mixtures [45] and H_2-O_2 coaxial injections [38]. The slight increment in the geometrical parameters of the flame that can be seen when T_{cf} becomes equal to 1223 K can be ascribed to the reduction in the ignition delay, and the fuel jet therefore reaches the autoignition condition closer to the nozzle outlet (the lift-off length reduces), which in turn leads to a small increment in the flame length (cf. Fig. 5) and, consequently, in the perimeter and the area.

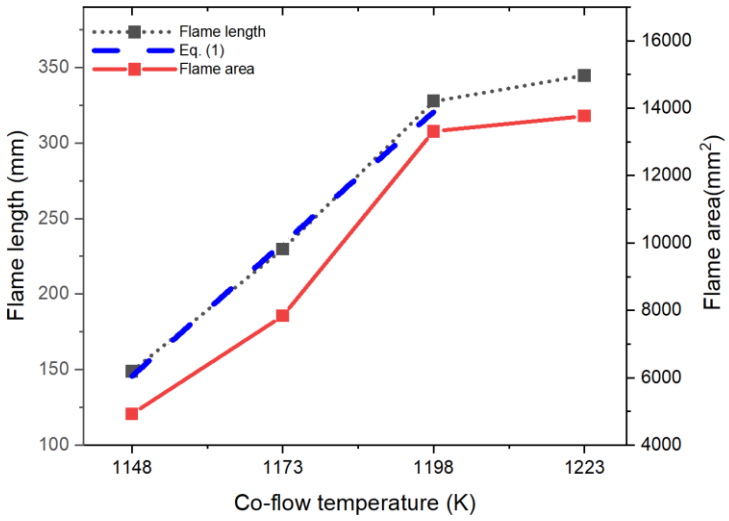


Figure 9. Flame length, flame length model based on Eq. (1) and flame area of ammonia gas for different co-flow temperatures (u_{cf} = 25 m/s, p_{inj} =1.9 bar).

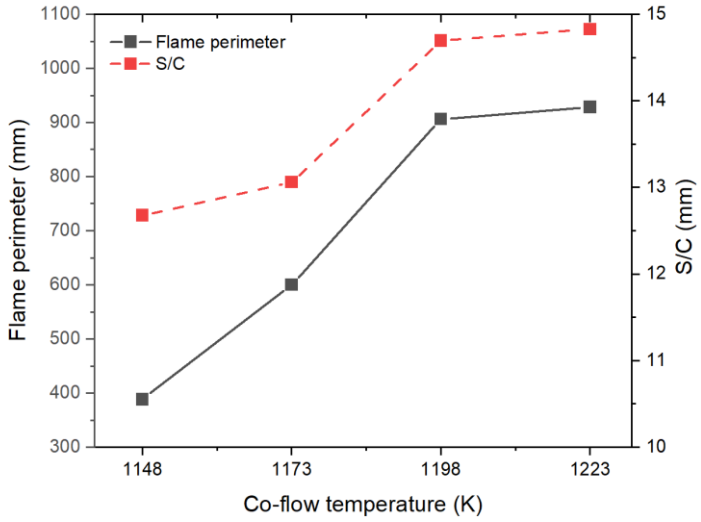


Figure 10. Perimeter and *S/C* of the ammonia flame for different co-flow temperatures (u_{cf} = 25 m/s, p_{inj} =1.9 bar).

Figures 11 and 12 compare characteristic parameters of the ammonia jet flame for different injection pressures. The experimental T_{cf} is 1223 K, and the different curves refer to two co-flow velocities equal to 23 m/s (continuous lines) and to 32 m/s (dashed lines). An increase in the co-flow velocity generally augments the turbulence of the co-flow field around the ammonia jet, and it therefore promotes heat transfer between the fuel and the co-flow field, thus leading to a growth in the length, the area, the perimeter and in the *S/C* of the jet flame. The rise in the ammonia jet speed (higher p_{inj}) obviously corresponds to an increment in the volumetric flowrate of ammonia: this enhances

the mixing rate with the oxygen that is present in the co-flow, and the temperature of the flame combustion rises, thus improving the diffusion of the ammonia jet gas and promoting chemical reactions. Furthermore, because of the increase in the jet momentum, the diffusion distance of the ammonia jet increases in both the axial and radial directions and leads to a change in the flame morphology.

However, when the jet pressure exceeds 2.2 bar, as reported in Figures 11-12, a rapid decline in the length, area, and perimeter of the ammonia flame can be noted. Indeed, a large amount of ammonia is injected into the co-flow field and it cannot be fully burned [46]. Therefore, there may be a large amount of unburned ammonia in the co-flow field, which could lead to a reduction in the length, area, and perimeter of the ammonia flame. However, the perimeter of the flame tends to reduce less than the area and length of the flame for high co-flow velocity values. Indeed, although the length and size of the flame reduce for an elevated co-flow velocity, due to incomplete combustion, the flame can be more wrinkled, due to the elevated u_{cf}, thus mitigating the reduction in the flame perimeter.

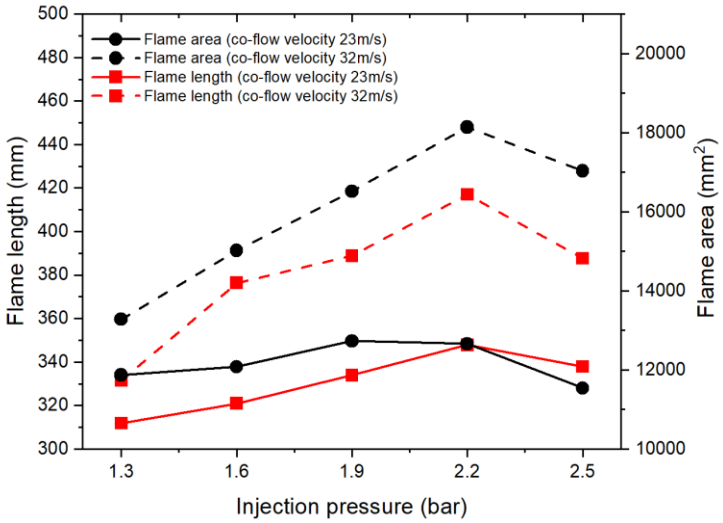


Figure 11. Length and area of the ammonia flame for different jet velocities ($T_{cf} = 1223$ K).

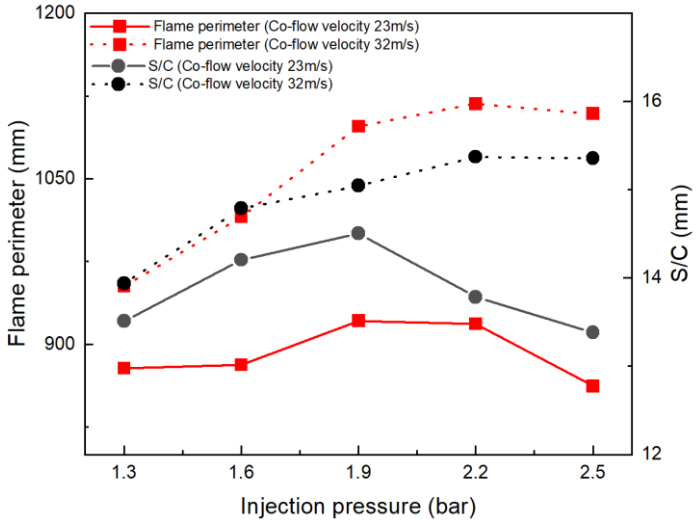


Figure 12. Perimeter and aspect ratio of the ammonia flame for different jet velocities (T_{cf} = 1223 K).

3.4 Autoignition point and ignition delay characteristics of an ammonia flame.

Figure 13 shows the ammonia autoignition location for different co-flow temperature values, considering a co-flow velocity equal to 25 m/s and an injection pressure of 1.9 bar. The autoignition point was assumed as the first flame spot that could be detected by the camera. As can be seen in Figure 13, the position of the autoignition point becomes closer to the nozzle outlet as the co-flow temperature increases. The fire cores from 1148 K to 1173 K are small, scattered and even unconnected, and they show a multi-point distribution accompanied by wrinkles. As the co-flow temperature increases, the fire cores gradually become concentrated, the fuzzy boundary disappears, and the fire core moves closer to the nozzle exit and becomes brighter. Indeed, the augmented co-flow temperature provides the ammonia jet with more energy, thus promoting autoignition and making the position of the autoignition point closer to the nozzle outlet. Figure 14 shows the pattern of the ignition delay with respect to the co-flow temperature for a fixed co-flow velocity and p_{inj}. The reported values, for which a discrepancy below 5% has been observed over three different acquisitions, were determined as intervals between the time instants at which the fuel solenoid valve opened and the first flame that occurred by subtracting the time required for the fuel to flow from the solenoid valve to the pipe outlet at a velocity of u_{inj}≈16.8 m/s (the distance between the solenoid valve and the fuel pipe outlet was available). The ignition delay of the ammonia jet decreases as T_{cf} increases. When the co-flow temperature is closer to 1148 K, there is still ammonia in the unstable

autoignition region (cf. Figure 8), and a rise in the co-flow temperature therefore helps to ensure combustion stability, which in turn leads to a pronounced drop in the ignition delay to T_{cf} = 1173 K. The injection pressure is in fact too high for the tested conditions to allow the ammonia to absorb enough energy from the co-flow at T_{cf} = 1148 K, and this leads to a high value of the flame lift height and to the presence of unburned ammonia. When T_{cf} rises to 1198 K, the fuel attains a stable flame lifting, and the ignition delay decreases even further. The energy exchange between the fuel and the co-flow at this temperature is sufficient to ensure a stable flame. Finally, when the co-flow temperature exceeds 1198 K, the ammonia flame is always stable, and the influence of the co-flow temperature on the ignition delay of ammonia is reduced. As mentioned above (cf. Table 2), when the co-flow temperature changes from 1123 K to 1223 K, the oxygen concentration reduces by about 5%, and its effect on the ignition delay is therefore negligible.

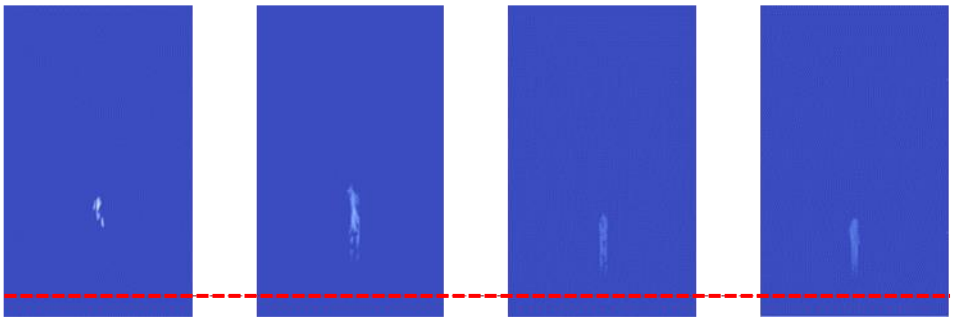


Figure 13. Location of the autoignition point of ammonia gas for different co-flow temperatures (u_{cf} = 25 m/s, p_{inj}=1.9 bar).

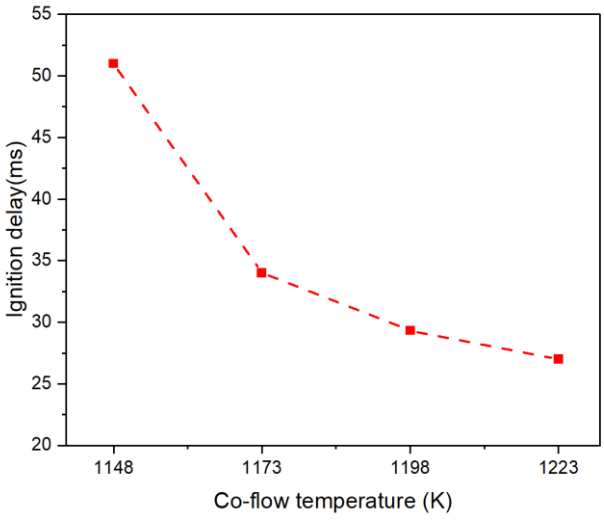


Figure 14. Ignition delay period of ammonia gas for different co-flow temperatures (u_{cf} = 25 m/s, p_{inj}=1.9 bar).

3.5 Normalized lift height and combustion stability

The normalized flame lift height, *H/d*, which corresponds to an average position of the flame, can be used to quantify the flame stability since it is sensitive to several flow and flame parameters, especially to the co-flow temperature [35]. Figure 15 compares the *H/d* of an ammonia jet flame for different co-flow temperatures. The experimental co-flow velocity is equal to 25 m/s, and the injection pressure is 1.9 bar. The normalized lift height of the flame of the ammonia diffusive combustion gradually decreases as the co-flow temperature augments, and the decreasing rate differs significantly for low and high co-flow temperatures. When the co-flow temperature is lower than 1173 K, *H/d* is particularly sensitive to T_{cf}, whereas the change in the co-flow temperature has less effect for T_{cf} >1173 K. Therefore, the normalized lift height of the flame shows a trend that is very similar to that of the ignition delay (cf. Figure 14). An augmented co-flow temperature even increases the flame stability of *H/d*, due to an enhanced heat exchange.

By using a controllable thermal atmosphere burner, such as the one employed in this work to study the autoignition of the turbulent flame, it has been shown that many fuels show a co-flow temperature threshold beyond which its influence on the normalized lift height of the flame drastically reduces [47]. The temperature threshold for the ammonia under the considered experimental conditions (u_{cf} =25 m/s, p_{inj}=1.9 bar) can be identified at T_{cf}= 1173 K, which corresponds to the knee for both the ignition delay (cf. Figure 14) and the flame *H/d* (cf. Figure 15).

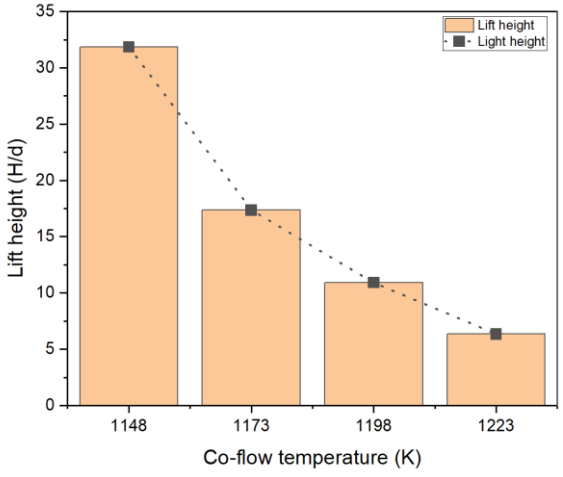


Figure 15. Normalized lift height of the ammonia flame for different co-flow temperatures (u_{cf} =25 m/s, p_{inj}=1.9 bar).

The velocity and injection pressure of a co-flow have important effects on the normalized lift height of ammonia [48]. Figure 16 compares the *H/d* trends of the flame with respect to the injection

pressure for different co-flow velocities. As already explained, the increase in the ammonia injection pressure increases the concentration of ammonia in the area near the fuel injection tube, thus leading to augmented local equivalence ratios, and autoignition is therefore not promoted and the ammonia flame settles further away from the injector tube outlet.

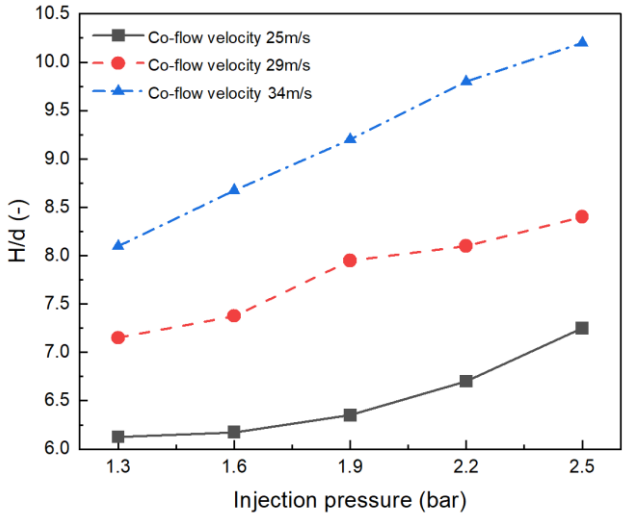


Figure 16. Normalized lift height versus injection pressure for different co-flow velocities (T_{cf} =1223 K).

A model for auto-ignited flames in high-velocity co-flows, which is suitable for interpreting the results in Figures 15 and 16, was developed in [49], where such a model was referred to as "large-scale mixing model". In that model, the normalized lift height was expressed as:

$$\frac{H}{d} \propto \tau_{ign,ad} \frac{(k_{st})^{\alpha}}{\tau'_{mix}{}^{1-\alpha}} \qquad (2)$$

where $\tau_{ign,ad}$ is the ignition delay, determined by means of CHEMKIN, under adiabatic stoichiometric conditions, k_{st} is the strain rate, α is a parameter in the [0,1] range, and τ'_{mix} is the mixing time scale of the large eddies. Strain rate k_{st} accounts for the effect of the interaction between the Kolmogorov eddies, which are the smallest eddies responsible for extinction, and the flame thickness [50]. When α = 1, a small-scale strain has the most important effect on *H/d,* which is therefore dominated by the Kolmogorov scale, while large-scale mixing controls the normalized lift height if α = 0. τ'_{mix} considers the effect of large eddies emanated by the fuel jet (the higher the fuel jet velocity is, the lower τ'_{mix}). These eddies, which are initially only constituted by pure fuel, then mix with the surrounding air. When the mixture reaches the autoignition condition, a flame edge is formed and is swept downstream. The air surrounding the flame is heated and becomes available to ignite the next mixture eddy arriving from the fuel nozzle side. The rapid formation

493 frequency and propagation of eddies allows the flame to remain stable and not to be blown out [51].
494 The flame strain rate in Eq. (2) can be estimated as

495 $$k_{st} \propto \frac{u_{inj}}{d}(Re_{co} \cdot f_M)^{0.5} \quad (3)$$

496 where u_{inj} is the fuel velocity, d is the injector pipe diameter, Re_{co} stands for the Reynolds number
497 of the co-flow, and f_M is defined as

498 $$f_M = \left[1 + \frac{1-M}{\left(\frac{d_{cf}}{d}\right)^2 M}\right]^{0.5} \quad (4)$$

499 In Eq. (4), d_{cf} is the diameter of the burner disk (equal to 100 mm) and M is the specific co-flow-to-
500 jet momentum flux ratio, which is defined as:

501 $$M = \left(\frac{u_{cf}}{u_{inj}}\right)^2 \frac{\rho_{cf}}{\rho_{inj}} \quad (5)$$

502 The large-scale mixing time, τ'_{mix}, in Eq. (2) can be expressed as

503 $$\frac{1}{\tau'_{mix}} \propto \frac{u_{inj}}{L_P}\left[1 + C\left(\frac{\Delta u}{u_{cf}}\right)\right] \quad (6)$$

504 where C is a positive coefficient that represents the degree of the shearing effect on the large-scale
505 mixing time, $\Delta u = u_{inj} - u_{cf}$, and L_p is the potential core length [52], which is evaluated as

506 $$\begin{cases} \frac{L_p}{d} = 4 + 12\left(\frac{u_{cf}}{u_{inj}}\right) & \text{if } u_{cf} < u_{inj} \\ \frac{L_p}{d} = 16 \cdot \left(\frac{u_{inj}}{u_{cf}}\right) & \text{if } u_{cf} > u_{inj} \end{cases} \quad (7)$$

507 The obtained experimental normalized lift height data have been replotted in Figure 17. A
508 satisfactory fit of the dashed-line is found for C=0.167 and α = 0 when the modified mixing-strain
509 model given by Eq. (2) is used. This means that the diffusive combustion of ammonia is controlled
510 by large-scale mixing in a high-temperature co-flow.
511

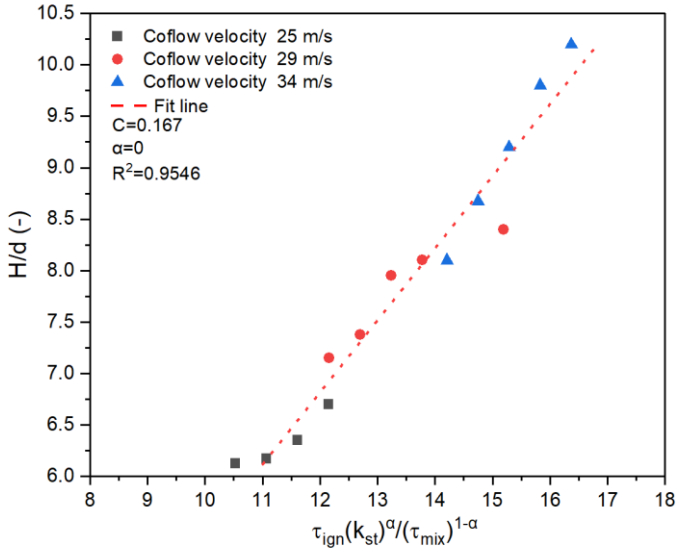


Figure 17. Modified mixing-strain model correlation of the normalized lift-off height for different co-flow velocities (T_{cf}=1223 K).

A measure of the flame stability of the diffusive combustion of ammonia can be obtained from the time-fluctuations of the flame normalized lift height. Such oscillations are reported in the left part of Figure 18 for different co-flow temperatures, and for a co-flow velocity and injection pressure equal to 25 m/s and 1.9 bar, respectively. As the co-flow temperature increases, the flame lift reduces and becomes more stable. This is also evident in the part on the right of Figure 18, where the standard deviation of *H/d* in the considered time interval, i.e. 260ms, is reported: it can be observed that the standard deviation dramatically reduces when the co-flow temperature increases. The burning flame diffusion becomes more pronounced for higher co-flow temperatures, because of both the faster flame speed and lower ignition delay, and the flame stability of ammonia diffusive combustion is improved. Indeed, when the co-flow temperature is high, the mixing process between the ammonia in the jet and the oxygen in the co-flow is accelerated, which is more conducive to the formation of a combustible gas mixture, thus making the combustion become more stable. Moreover, there is no obvious multi-point autoignition phenomenon.

Instead, when the co-flow temperature is low, the combustion of the ammonia jet is somewhat unstable and is accompanied by a sharp burst sound (this burst sound disappears as soon as the co-flow temperature exceeds a certain value). The flame front is uneven, the shape is very irregular, and the direction and speed of the flame front change frequently in the combustion process: unburned ammonia can be diffused and heated from all directions, and the resulting small explosions

emit sharp pressure pulses that cause ringing.

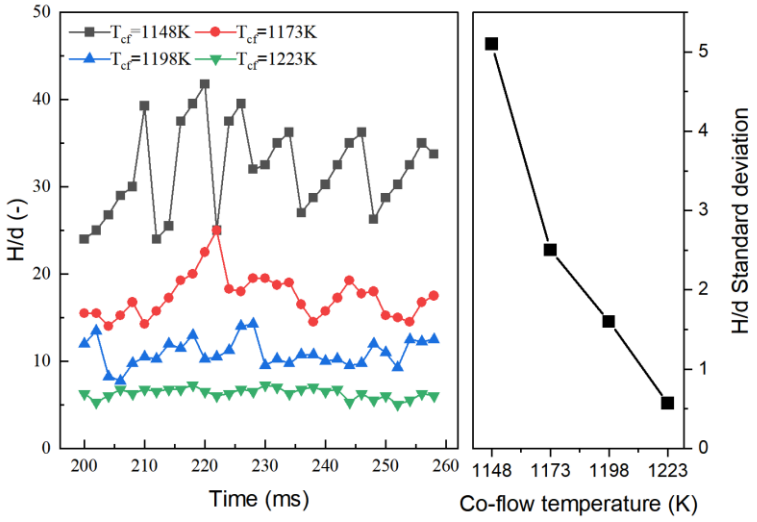


Figure 18. Normalized lift height time fluctuations for different co-flow temperatures (u_{cf} =25 m/s, p_{inj}=1.9 bar).

The *H/d* fluctuations, with respect to time, for different injection pressures are reported in Figure 19 (u_{cf} =25 m/s, T_{cf}=1223 K). The standard deviation of the normalized lift height of the flame in the considered time interval increases as the injection pressure increases. A higher pressure leads to larger fluctuations, due to the intensified turbulence disturbance caused by the augmented Reynolds number of the fuel. The injection velocity rises as the injection pressure increases, and the flame morphology continuously changes from lift-off to blow-off: the ammonia lifted flame shows a critical autoignition (CA) behavior for p_{inj} = 2.5 bar, which is represented by continuous flame extinctions and reignitions [53]. It has been verified, on the basis of an analysis of different working conditions, that the stability of the flame can be quantitatively assessed by means of the standard deviation of the normalized lift-off length: as can be inferred from Figures 18 and 19, by considering the results reported in Figures 7 and 8, when the *H/d* standard deviation is clearly below 2, the flame can be considered stable.

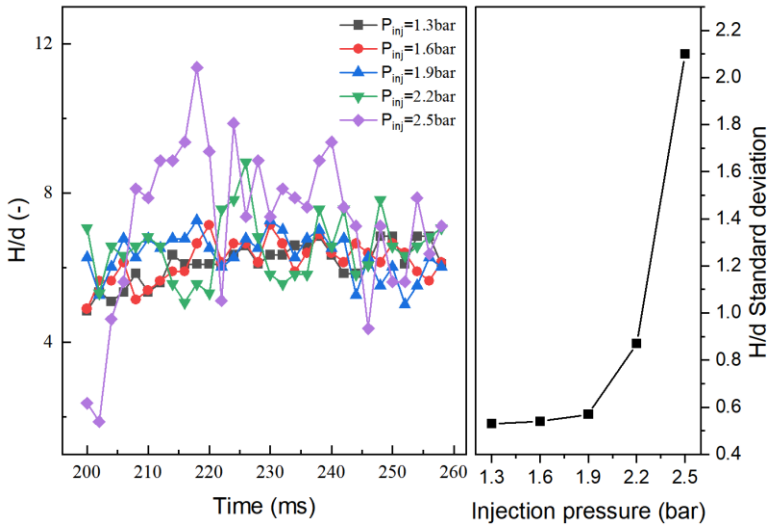


Figure 19. Normalized lift height time fluctuations for different injection pressures (u_{cf} =25 m/s, T_{cf}=1223 K).

Blow off occurs for ammonia at p_{inj}=2.5 bar and u_{cf}= 34 m/s as both the co-flow velocity and injection pressure increase, as reported in Figure 20, where some consecutive flame photos have been reported over the 200-260 ms range after the beginning of the fuel flow: a critical autoignition behavior, featuring the repetition of extinctions and reignition, occurs. The burnt gas could in fact induce a local acceleration in the streamwise velocity, due to buoyancy, and this could lead to a blowout. Autoignition can again occur when the local velocity decelerates, as a result of the mitigation of the buoyancy effect [53].

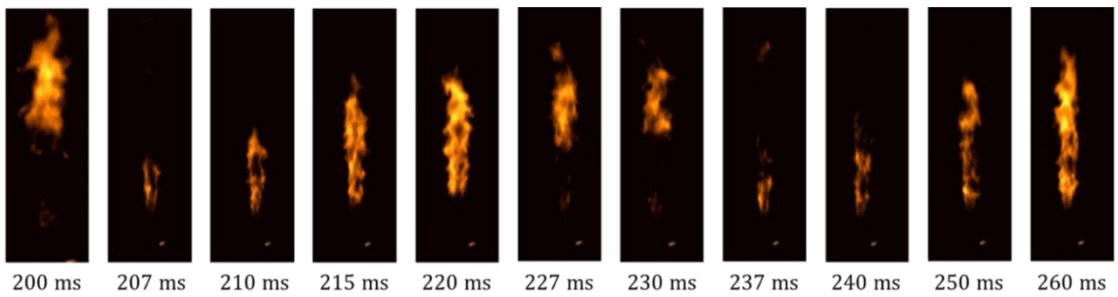


Figure 20. Fluctuation and reignition phenomenon of the flame over the 200-260 ms range after the beginning of the fuel flow. (T_{cf} = 1223 K, p_{inj}=2.5 bar, u_{cf} =34 m/s)

4. Conclusions

The combustion characteristics and flame stability of an ammonia turbulence jet diffusion flame have been investigated for different co-flow temperatures, co-flow velocities, and jet velocities.

The ammonia flame appears orange, with sporadic red zones. When T_{cf} <1148 K (u_{cf} = 25 m/s, p_{inj} = 1.9 bar), a stable lifting flame is not achieved, resulting in low brightness. Extinctions and

reignitions are common at T_{cf} = 1173 K, and stability increases significantly when $T_{cf} \geq$ 1198 K.

Increasing co-flow velocity and injection pressure hinders ammonia combustion. Higher co-flow temperature (T_{cf} > 1223 K) is necessary for a stable lifting flame at greater co-flow velocity (34 m/s) and injection pressure (2.5 bar).

Flame characteristics like length, area, and perimeter increase with co-flow temperature while they first increase and then decrease with the injection pressure. If s$p_{inj} > 2.2$ bar ammonia combustion is incomplete, and flame geometrical characteristics reduce.

The distance from the position of the autoignition point to the nozzle outlet and ignition delay both decrease with rising T_{cf}, notably from 1148 K to 1223 K, with the most significant reduction observed at $T_{cf} \leq$ 1173 K. Normalized lift height decreases as co-flow temperature rises but, for T_{cf} ≥ 1173 K, the co-flow temperature impact on *H/d* reduces.

The normalized lift-off length data satisfactorily fit a modified mixing-strain model, thus showing that the combustion is controlled by large-scale mixing.

Flame stability notably improves with higher co-flow temperatures, evidenced by reduced flame fluctuations over time. A standard deviation of the normalized lift height below 2 indicates a stable flame.

5. Funding

The authors would like to acknowledge the Natural Science Foundation of China [grant numbers T2241003], the Shanghai Science and Technology Program (grant numbers 22ZR1463000) and the Chinese Ministry of Science and Technology (grant numbers G2023133001L) for funding this study.

6. References

[1] P.G. Grimes Energy depot fuel production and utilization SAE Trans, 74 (1966), pp. 281-326.

[2] D.Richards, R.W. Hender OTEC produced ammonia: an alternative fuel 8th ocean energy conf. (1981), pp. 665-673.

[3] T.A. Czuppon, S.A. Knez, J.M. Rovner Ammonia Kirk-othmer encycl. Chem. Technol (fourth ed.), Wiley, New York (1992), pp. 638-691

[4] V. Dias, M. Pochet, F. Contino, H. Jeanmart Energy and economic costs of chemical storage Front Mech Eng, 6 (2020), p. 21

[5] Cornelius W, Huellmantel L W, Mitchell H R. Ammonia as an engine fuel[J]. SAE Transactions, 1966: 300-326

[6] Gray Jr J T, Dimitroff E, Meckel N T, et al. Ammonia fuel—engine compatibility and combustion[J]. SAE Transactions, 1967: 785-807.

[7] Mørch C S, Bjerre A, Gøttrup M P, et al. Ammonia/hydrogen mixtures in an SI-engine: Engine performance and analysis of a proposed fuel system[J]. Fuel, 2011, 90(2): 854-864.

[8] Ge Y T, Fsadni A M, Wang H S. Bubble dissolution in horizontal turbulent bubbly flow in domestic central heating system[J]. Applied energy, 2013, 108: 477-485.

[9] Frigo S, Gentili R. Analysis of the behaviour of a 4-stroke Si engine fuelled with ammonia and hydrogen[J]. International Journal of Hydrogen Energy, 2013, 38(3): 1607-1615.

[10] Mounaïm-Rousselle C, Bréquigny P, Dumand C, et al. Operating limits for ammonia fuel spark-ignition engine[J]. Energies, 2021, 14(14): 4141.

[11] Valera-Medina A, Xiao H, Owen-Jones M, et al. Ammonia for power[J]. Progress in Energy and combustion science, 2018, 69: 63-102.

[12] Liu S, Lin Z, Zhang H, et al. Impact of ammonia addition on knock resistance and combustion performance in a gasoline engine with high compression ratio[J]. Energy, 2023, 262: 125458.

[13] Hideaki Kobayashi, Akihiro Hayakawa, K.D. Kunkuma A. Somarathne, Ekenechukwu C. Okafor,Science and technology of ammonia combustion,Proceedings of the Combustion Institute,Volume 37, Issue 1, 2019, Pages 109-133,

[14] A Valera-Medina, H Xiao, M Owen-Jones, W.I.F. David, P.J. Bowen. Ammonia for power. Progress in Energy and Combustion Science. 2018; 69: 63-102.

[15] Ebrahim Nadimi, Grzegorz Przybyła, Michał T. Lewandowski, Wojciech Adamczyk, Effects of ammonia on combustion, emissions, and performance of the ammonia/diesel dual-fuel compression ignition engine, Journal of the Energy Institute, Volume 107, 2023, 101158.

[16] Long Liu, Jie Wu, Haifeng Liu, Yue Wu, Yang Wang, Study on marine engine combustion and emissions characteristics under multi-parameter coupling of ammonia-diesel stratified injection mode, International Journal of Hydrogen Energy, Volume 48, Issue 26, 2023, Pages 9881-9894,

[17] Niels Førby, Thomas B. Thomsen, Rasmus F. Cordtz, Frantz Bræstrup, Jesper Schramm,Ignition and combustion study of premixed ammonia using GDI pilot injection in CI engine, Fuel, Volume 331, Part 1,2023,125768.

[18] Gross, Christopher W., and Song-Charng Kong. "Performance characteristics of a compression-ignition engine using direct-injection ammonia–DME mixtures." Fuel 103 (2013): 1069-1079.

628 [19] Ferrari A, Vento O. Thermal effects on Common Rail injection system hydraulic
629 performance[J]. International Journal of Engine Research, 2023: 14680874231162412.
630 [20] Ferrari A, Novara C, Vento O, et al. A novel fuel injected mass feedback-control for single and
631 multiple injections in direct injection systems for CI engines[J]. Fuel, 2023, 334: 126670.
632 [21] Jin Z, Vento O, Zhang T, et al. Numerical-experimental optimization of the common-feeding
633 injection system concept for application to light-duty commercial vehicles[J]. Journal of Energy
634 Resources Technology, 2021, 143(12): 122304.
635 [22] Ferrari, A., Jin, Z., Vento, O., Zhang, T. An injected quantity estimation technique based on
636 time-frequency analysis. Control Engineering Practice 116 (2021): 104910.
637 [23] Ferrari, Alessandro, Pietro Pizzo, and Oscar Vento. "Investigation of a GDI injector with an
638 innovative flowmeter for high-pressure transient flows." International Journal of Engine Research
639 24.9 (2023): 4287-4296.
640 [24] Jun Li, Hongyu Huang, Noriyuki Kobayashi, Chenguang Wang, Haoran Yuan, Numerical study
641 on laminar burning velocity and ignition delay time of ammonia flame with hydrogen addition,
642 Energy, Volume 126, 2017, Pages 796-809.
643 [25] Olivier Mathieu, Eric L. Petersen,Experimental and modeling study on the high-temperature
644 oxidation of Ammonia and related NOx chemistry, Combustion and Flame, Volume 162, Issue 3,
645 2015, Pages 554-570.
646 [26] Giovanni Battista Ariemma, Giancarlo Sorrentino, Raffaele Ragucci, Mara de Joannon, Pino
647 Sabia, Ammonia/Methane combustion: Stability and NOx emissions, Combustion and Flame,
648 Volume 241, 2022, 112071.
649 [27] A. Karan, G. Dayma, C. Chauveau, F. Halter Experimental study and numerical validation of
650 oxy-ammonia combustion at elevated temperatures and pressures Combust Flame, 236 (2022),
651 Article 111819.
652 [28] A. Hayakawa, T. Goto, R. Mimoto, Y. Arakawa, T. Kudo, H. Kobayashi Laminar burning
653 velocity and Markstein length of ammonia/air premixed flames at various pressures
654 Fuel, 159 (2015), pp. 98-106.
655 [29] Wu, Zhijun, et al. "Numerical investigation on the flame propagation process of
656 ammonia/hydrogen blends under engine-related conditions." International Journal of Hydrogen
657 Energy 60 (2024): 1041-1053.

[30] Hu X, Luo C, Chen X, et al. Study on flame propagation and inherent instability of hydrogen/ammonia/air mixture[J]. Fuel, 2024, 357: 129848.

[31] Yu Xia, Genya Hashimoto, Khalid Hadi, Nozomu Hashimoto, Akihiro Hayakawa, Hideaki Kobayashi, Osamu Fujita,Turbulent burning velocity of ammonia/oxygen/nitrogen premixed flame in O2-enriched air condition,Fuel, Volume 268.

[32] H. Kobayashi, A. Hayakawa, K.K.A. Somarathne, E.C. Okafor Science and technology of ammonia combustion Proc Combust Inst, 37 (1) (2019), pp. 109-133

[33] Yang W, Dinesh K K J R, Luo K H, et al. Direct numerical simulation of turbulent premixed ammonia and ammonia-hydrogen combustion under engine-relevant conditions[J]. International Journal of Hydrogen Energy, 2022, 47(20): 11083-11100.

[34] Ji, Meng, et al. Combustion and Emission Characteristics of Ammonia Jet Flames, Based on a Controllable Activated Thermal Atmosphere. No. 2023-01-1645. SAE Technical Paper, 2023.

[35] R. Cabra, J.-Y. Chen, R.W. Dibble, A.N. Karpetis, R.S. Barlow, Lifted methane-air jet flames in a vitiated coflow, Combustion and Flame, Volume 143, Issue 4, 2005, Pages 491-506.

[36] Zhang E, Gong Y, Deng J, Hu Z, Jiang C, Wu Z, Li L. Cyclic Variations of Argon Power Cycle Engine with Fuel of Hydrogen. SAE 2017-01-2409.

[37] Z. Wu, W. Xie, E. Zhang, et al. Investigation of Flame Characteristics of Hydrogen Jet Issuing into a Hot Vitiated Nitrogen/Argon/Carbon Dioxide Co-flow. International Journal of Hydrogen Energy, 2019, 44(52): 28357-28370.

[38] Zhijun Wu, Yang Yu, Wei Xie, Zheng Liu, Liguang Li, Jun Deng, Optimization of the flame characteristics of H2-O2 coaxial injection applied to hydrogen-fueled argon cycle engines, International Journal of Hydrogen Energy, Volume 46, Issue 27, 2021, Pages 14780-14789.

[39] Qin, Q., Wu, Z., and Ferrari, A. Study on Lifted Flame Stabilization Under Different Background Pressures." ASME. J. Thermal Sci. Eng. Appl. 2022; 14(2): 021006.

[40] Gregory P. Smith, David M. Golden, Michael Frenklach, Nigel W. Moriarty, Boris Eiteneer, Mikhail Goldenberg, C. Thomas Bowman, Ronald K. Hanson, Soonho Song, William C. Gardiner, Jr., Vitali V. Lissianski, and Zhiwei Qin http://www.me.berkeley.edu/gri_mech/

[41] Akihiro Hayakawa, Takashi Goto, Rentaro Mimoto, Yoshiyuki Arakawa, Taku Kudo, Hideaki Kobayashi, Laminar burning velocity and Markstein length of ammonia/air premixed flames at various pressures,Fuel,Volume 159,2015,Pages 98-106.

688 [42] Hayakawa A, Goto T, Mimoto R, et al. NO formation/reduction mechanisms of ammonia/air
689 premixed flames at various equivalence ratios and pressures[J]. Mechanical Engineering Journal,
690 2015, 2(1): 14-00402-14-00402.
691 [43] Liang B, Gao W, Zhang K, et al. Ammonia-air combustion and explosion characteristics at
692 elevated temperature and elevated pressure[J]. International Journal of Hydrogen Energy, 2023.
693 [44] Delichatsios M A. Transition from momentum to buoyancy-controlled turbulent jet diffusion
694 flames and flame height relationships[J]. Combustion and Flame, 1993, 92(4): 349-364.
695 [45] Gong Y, Zhan Y, Deng J, et al. Experimental and numerical study on combustion characteristics
696 of hydrogen-argon jet in a hot vitiated Co-flow[R]. SAE Technical Paper, 2018.
697 [46] Choi B C, Kim K N, Chung S H. Autoignited laminar lifted flames of propane in coflow jets
698 with tribrachial edge and mild combustion[J]. Combustion and Flame, 2009, 156(2): 396-404.
699 [47] Wu Z, Bao T, Zhang Q, et al. Experimental study on spray combustion characteristics of
700 gasoline–diesel blended fuel in a controllable active thermo-atmosphere[J]. Fuel, 2014, 135: 374-
701 379.
702 [48] S.R. Turns, R.B. Bandaru, Oxides of Nitrogen Emissions from Turbulent Hydrocarbon/Air Jet
703 Diffusion Flames: Final Report-Phase II, Gas Research Institute, September 1992.
704 [49] Liu G, Li S, Wu Y. Effects of coflow velocity on the lift-off characteristics of autoignited jet
705 flame in hot air coflow[J]. Combustion and Flame, 2024, 259: 113124.
706 [50] Liu G, Li S. Lift-off height of autoignited jet flame in hot air coflow with different O2
707 contents[J]. Combustion and Flame, 2022, 242: 112144
708 [51] Lawn C J. Lifted flames on fuel jets in co-flowing air[J]. Progress in Energy and Combustion
709 Science, 2009, 35(1): 1-30
710 [52] J. Beér, N. Chigier, Combustion Aerodynamics, Krieger Publishing Company, London, U.K.,
711 1972.
712 [53] Choi, B. C., Chung, S. H. (2010). Autoignited laminar lifted flames of methane, ethylene,
713 ethane, and n-butane jets in coflow air with elevated temperature. Combustion and flame, 157(12),
714 2348-2356.